Energy Band Gap and Optical Transition of Metal Ion Modified Double Crossover DNA Lattices
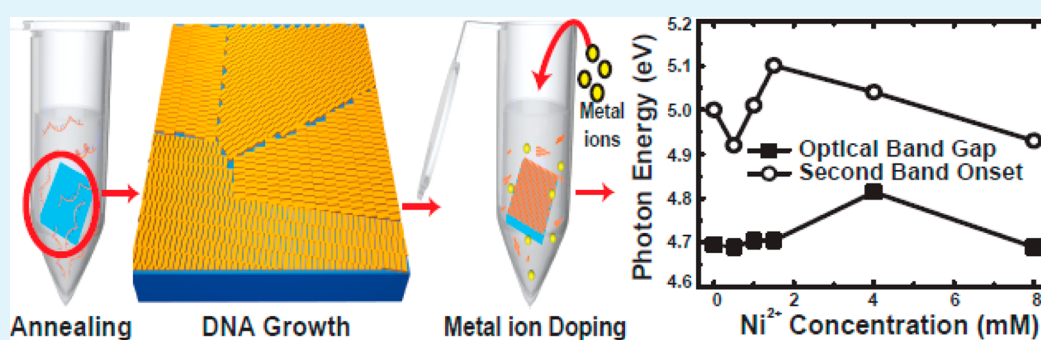
Sreekantha Reddy Dugasani,[†,§] Taewoo Ha,[‡,§] Bramaramba Gnapareddy,[†] Kyujin Choi,[‡] Junwye Lee,[†] Byeonghoon Kim,[†] Jae Hoon Kim,*[,‡] and Sung Ha Park*[,†]

[†]Department of Physics and Sungkyunkwan Advanced Institute of Nanotechnology (SAINT), Sungkyunkwan University, Suwon 440-746, Korea

[‡]Department of Physics, Yonsei University, Seoul 120-749, Korea

Ⓢ Supporting Information

ABSTRACT: We report on the energy band gap and optical transition of a series of divalent metal ion (Cu^{2+}, Ni^{2+}, Zn^{2+}, and Co^{2+}) modified DNA (M−DNA) double crossover (DX) lattices fabricated on fused silica by the substrate-assisted growth (SAG) method. We demonstrate how the degree of coverage of the DX lattices is influenced by the DX monomer concentration and also analyze the band gaps of the M−DNA lattices. The energy band gap of the M−DNA, between the lowest unoccupied molecular orbital (LUMO) and the highest occupied molecular orbital (HOMO), ranges from 4.67 to 4.98 eV as judged by optical transitions. Relative to the band gap of a pristine DNA molecule (4.69 eV), the band gap of the M−DNA lattices increases with metal ion doping up to a critical concentration and then decreases with further doping. Interestingly, except for the case of Ni^{2+}, the onset of the second absorption band shifts to a lower energy until a critical concentration and then shifts to a higher energy with further increasing the metal ion concentration, which is consistent with the evolution of electrical transport characteristics. Our results show that controllable metal ion doping is an effective method to tune the band gap energy of DNA-based nanostructures.

KEYWORDS: DNA, lattices, M−DNA, energy band gap, HOMO−LUMO, optical transition

1. INTRODUCTION

Deoxyribonucleic acid (DNA) is one of the most promising biomolecules for use in the fabrication of designed nanostructures and has many innovative features including self-assembly, programmability, molecular recognition, and designable nanoscale structures.[1] These exceptional features of DNA allow for the employment of highly versatile binding strategies for the creation of complex DNA nanostructures in one, two, and even three dimensions.[2−5] The study of structural DNA nanotechnology is highly multidisciplinary and encompasses natural sciences and traditional engineering as well as computer science for the utilization of DNA to realize a new class of physical, chemical, biological, and medical devices and sensors. This particular field benefits from the possibility to use designed nanoscale templates, which may allow for smarter, faster, and more energy-efficient fabrication approaches compared to conventional semiconductor-based technologies. Recently, several experimental and theoretical works have discussed the

feasibility of such DNA-based materials and devices.[6−15] In view of the great potential for application in optoelectronics, nanobiosensors, nanoelectronics, and spintronics, we search for a new methodology to improve the electronic and optical properties of DNA-based nanostructures based on the doping of divalent metal ions such as copper, nickel, zinc, and cobalt ions (Cu^{2+}, Ni^{2+}, Zn^{2+}, and Co^{2+}). A broad range of tunability would enable promising applications in bioengineering, nanoelectronics, and biosensor architectures.

Although several reports have addressed the optical properties of single- and double-stranded DNA molecules in a solution phase, there have been certain limitations to determine the energy band gap of DNA thin films due to the amorphous nature of DNA molecules in water-based buffers containing
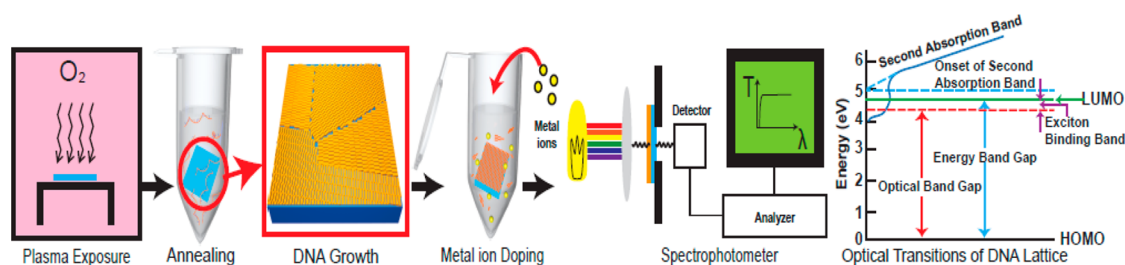
Figure 1. Schematics of the experimental procedure and the optical transitions of the 2D DNA lattice. O_2 plasma treatment on a fused silica substrate, DNA annealing along with the substrate, DNA lattice growth on the substrate, metal ion modification on the DNA lattices, and measurement by the spectrophotometer. Last schematic represents the optical transitions of 2D DNA lattice.

chemicals and counterions. Consequently, we attempted to grow a crystalline DNA monolayer made of artificially designed DNA building blocks with uniform duplex DNA thickness on a substrate in order to measure their optical properties in the dry phase. We used a glass substrate but soon realized that the glass absorption in the 250–350 nm wavelength range was very similar to the absorption of DNA molecules. To overcome this problem, we tried to grow DNA lattices on fused silica using the substrate-assisted growth (SAG) method.[16–18] Transparent fused silica exhibits fundamental absorption below 190 nm and transmits 90% of light above 200 nm, thereby providing favorable conditions for the band gap analysis of DNA lattices. Herein, we report double crossover (DX) lattice coverage as a function of DNA monomer concentration in order to study the DNA growth mechanism on fused silica and the optical characteristics of the resulting polycrystalline DX lattices coordinated with four different metal ions (Cu^{2+}, Ni^{2+}, Zn^{2+}, and Co^{2+}). Subsequently, we conducted direct measurements to identify the energy band gaps and optical transitions with a standard UV–vis–NIR spectrophotometer (Cary 5G).

2. EXPERIMENTAL PROCEDURE

The oxygen (O_2) plasma exposure process has been used extensively for substrate surface cleaning and/or functionalization. The treatment of the fused silica with O_2 plasma introduces functional groups which are mainly the silanol groups (SiOH). These groups change the surface properties of the fused silica from being hydrophobic to hydrophilic. Several parameters can affect the physical characteristics of plasma and subsequently affect the surface chemistry obtained by plasma modification. Optimum processing parameters, such as gas flow rate, treatment power, generation time, and operating pressure, are dependent on the substrate; however, system parameters, such as electrode location, reactor design, gas inlets, and vacuum level, are set by the design of the plasma equipment. This broad range of tunable parameters offers greater control over the plasma process compared to higher-energy radiation processes. An O_2 plasma cleaner (Femto Science; Gyeonggi, Korea) was used in the present study. The oxygen plasma process is conducted at a power of 50 W, a base pressure of 5×10^{-2} Torr, an oxygen flow rate of 45 SCCM, a working oxygen pressure of 7.8×10^{-1} Torr, and a plasma generation time of 10 min for each side of the substrate. O_2 plasma is exposed to both sides of a fused silica. If this is not done, it can be difficult to identify the DNA-grown side of the samples due to the transparent nature of the substrates.

Synthetic oligonucleotides purified by high performance liquid chromatography (HPLC) were purchased from BIONEER (Daejeon, Korea). Complexes were formed by mixing a $1 \times$ TAE/Mg^{2+} (40 mM Tris base, 20 mM acetic acid, 1 mM EDTA (pH 8.0), and 12.5 mM magnesium acetate) buffer solution which contained an equimolar mixture of eight different DX strands. For annealing, the fused silica substrate and the DNA strands were inserted into an AXYGEN tube with a total sample volume of 250 μL. This was then placed in a

Styrofoam box with 2 L of boiling water and cooled slowly from 95 to 25 °C over a period of at least 24 h to facilitate hybridization. During annealing, the DX strands form polycrystalline DX lattices on the substrate which eventually completely cover the fused silica surface. We also prepared a sample with a DX concentration of 50 nM in solution, which is well above the saturation concentration (20 nM) required for full coverage of the DX lattices.

After growing DX thin lattices on the fused silica substrate, the appropriate amount of copper ion solution [$Cu(NO_3)_2$] (2, 4, 6, 8, and 10 mM), nickel ion solution [$NiCl_2$] (0.5, 1, 1.5, 4, and 8 mM), zinc ion solution [$ZnCl_2$] (1, 1.5, 2, and, 4 mM), or cobalt ion solution [$CoCl_2$] (1, 1.5, 2, and 4 mM) was added and then incubated at room temperature for 24 h.

For AFM imaging, a substrate-assisted grown DNA sample was placed on a metal puck using instant glue. An amount of 30 μL of the $1 \times$ TAE/Mg^{2+} buffer was then pippetted onto the substrate, and another 10 μL of the $1 \times$ TAE/Mg^{2+} buffer was dispensed onto the AFM tip (NP-S10, Veeco Inc., USA). AFM images were obtained using a Multimode Nanoscope (Veeco Inc., USA) in the liquid tapping mode.

Measurements of optical transmission in the near-infrared, visible, and ultraviolet regions (wavelengths between 3300 and 175 nm) were carried out with a Varian Cary 5G spectrophotometer. The spectrophotometer was equipped with two light sources: a deuterium arc lamp (NIR and visible) and a quartz W-halogen lamp (UV). It also has two detectors: a cooled PbS detector for the NIR region and a photomultiplier tube for the visible and UV regions. The spectrophotometer measured the frequency-dependent light intensity passing either through a vacuum or through a sample. The present investigation was focused on the wavelength region between 1200 and 190 nm.

3. RESULTS AND DISCUSSION

A DX DNA lattice was adopted for this study.[3] Two repeating DX tiles (shown in the Supporting Information, Figure S1 and Tables S1 and S2) were used for the construction of the 2D lattices on a given substrate (sample preparation is explained below). A single unit of the DX tile is organized such that two crossover junctions and two parallel duplexes are tied up by the junctions. Generally, two different annealing methods can be used for the fabrication of DX lattices. While the conventional free-solution method has been more commonly used historically, the SAG method has been used more often recently. In this study, we adopt the latter approach to fabricate a DX lattice over a given substrate. We opted for the SAG method because the free-solution method is limited in its ability to grow relatively large DNA lattices[19] and also has issues relating to coverage control on a given substrate. During the SAG process, DNA crystallization (including random tile seeding, nucleation, and lattice growth) was successfully achieved. Annealing resulted in polycrystalline DX lattices with complete coverage as controlled by the concentration of

17600

dx.doi.org/10.1021/am503614x | *ACS Appl. Mater. Interfaces* 2014, 6, 17599–17605

the DX tiles. O_2 plasma treated fused silica was used as the substrate because its large band gap and wide transmission range allow for precise determination of the DNA band gap. Figure 1 shows a schematic for the overall processing and measurement procedures including O_2 plasma exposure to fused silica, DNA lattice growth, metal ion incubation, optical spectrophotometry, and the optical transitions of 2D DNA lattices.

The DX monomer concentration (C_m) is roughly proportional to the lattice coverage on a given substrate up to a saturation concentration (C_s). Eventually, the lattice coverage remains unchanged above C_s. To demonstrate the coverage dependence of C_m, 2D DX lattices were annealed at different DX C_m quantities. DX lattices were fabricated from DX tiles consisting of two adjacent duplex DNA molecules connected by two crossover junctions. To ensure accuracy and reliability, four physical conditions were fixed during the fabrication process: substrate size (5 mm × 5 mm), total volume of the DNA sample (250 μL), annealing temperature (from 95 to 25 °C), and annealing time (24 h). Different quantities of C_m were used.

The AFM images of the coverage dependence are shown in Figure 2. The DX lattices start to grow on the fused silica at a threshold concentration (C_{th}) of ~2 nM, while full coverage was reached at a C_s of ~20 nM. Figures 2(e and f) show fused silica substrates fully covered with monolayer 2D DX lattices. The yellow dotted lines indicate the DX lattice boundaries. The insets in the bottom left in Figures 2(e and f) are the noise-filtered 2D spectrum images according to fast Fourier transform and show the periodicity of the unit DX tiles (12 nm × 4 nm) over a scan size of 80 nm × 80 nm. Beyond the critical C_s, the coverage ratio of the DX lattices is unchanged with C_m; the excess DX tiles remain inside the test tube. Stripes (dark and bright regions) appear in most of the AFM images and are likely caused by the uneven surface roughness of the fused silica substrates. Although uneven and rough, individual DX building blocks were clearly observed. In the SAG method, nucleation of DNA molecules on the substrate occurs slightly below 10 nM; this is significantly lower than what is observed in the conventional free-solution case (nucleation at 40 nM). This was due to the catalytic behavior of the substrate, by which the Coulombic forces between the substrate and DNA strands pay a portion of the entropic cost of DNA crystallization.[17] This force creates a higher DNA molecular density close to the substrate, compared to the rest of the solution, and provides appropriate conditions for DNA crystallization.

Four different divalent metal ions (Cu^{2+}, Ni^{2+}, Zn^{2+}, and Co^{2+}), at various concentrations, were introduced into the DX polycrystalline structures fabricated on fused silica by the SAG method. The resulting DNA base pairings were highly dependent on the pH of a physiological 1× TAE/Mg^{2+} buffer. The metal ions were added to the DNA buffer solution after annealing the DX lattices on the substrate in order to avoid structural deformation of the DX lattices with varying ion concentrations.[20] In view of this observation, we altered our procedure such that metal ions were added after hybridization in order to maintain deformation-free DX lattices on the substrate. The experimental schematics of this procedure are shown in Figure 1. For consistency, the other circumferential parameters, i.e., the thermal energy, controlled by the annealing temperature ranging between 95 and 25 °C and the annealing time of 24 h; the electrostatic interaction between the substrate and the DNA molecules over the substrate size of 5 mm × 5
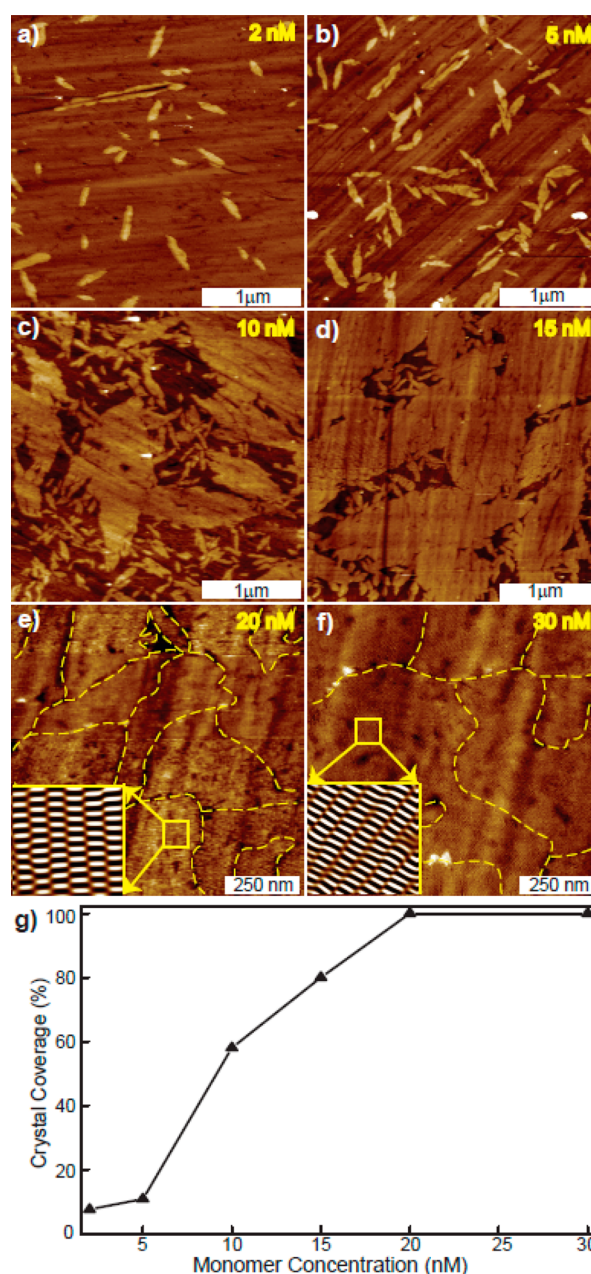

Figure 2. Analysis of DX lattice coverage on fused silica as a function of DX DNA monomer concentration in solution. (a−f) AFM images of DX lattices at various monomer concentrations (2, 5, 10, 15, 20, and 30 nM) grown by the substrate-assisted growth method. The insets (e, f) are the noise-filtered 2D spectra (scan size, 80 nm × 80 nm) by fast Fourier transform which show the periodicity of the lattices. (g) DX lattice coverage (%) controlled by DNA monomer concentration.

mm; the total sample volume of 250 μL in a test tube; and the DNA concentration (50 nM), were all fixed during the annealing process. The concentrations of Cu^{2+}, Ni^{2+}, Zn^{2+}, and Co^{2+} were varied. Figure 3 shows AFM images of these samples: Figures 3(a and b) correspond to copper ion concentrations [Cu^{2+}] of 4 and 8 mM, denoted as Cu4 and Cu8; Figures 3(c and d) correspond to [Ni^{2+}] of 1 and 8 mM, denoted as Ni1 and Ni8; Figures 3(e and f) correspond to [Zn^{2+}] of 1 and 4 mM, denoted as Zn1 and Zn4; and Figures 3(g and h) correspond to [Co^{2+}] of 1 and 2 mM, denoted as Co1 and Co2, respectively. The yellow dotted line in the AFM images indicates the DX lattice boundaries. The insets in the
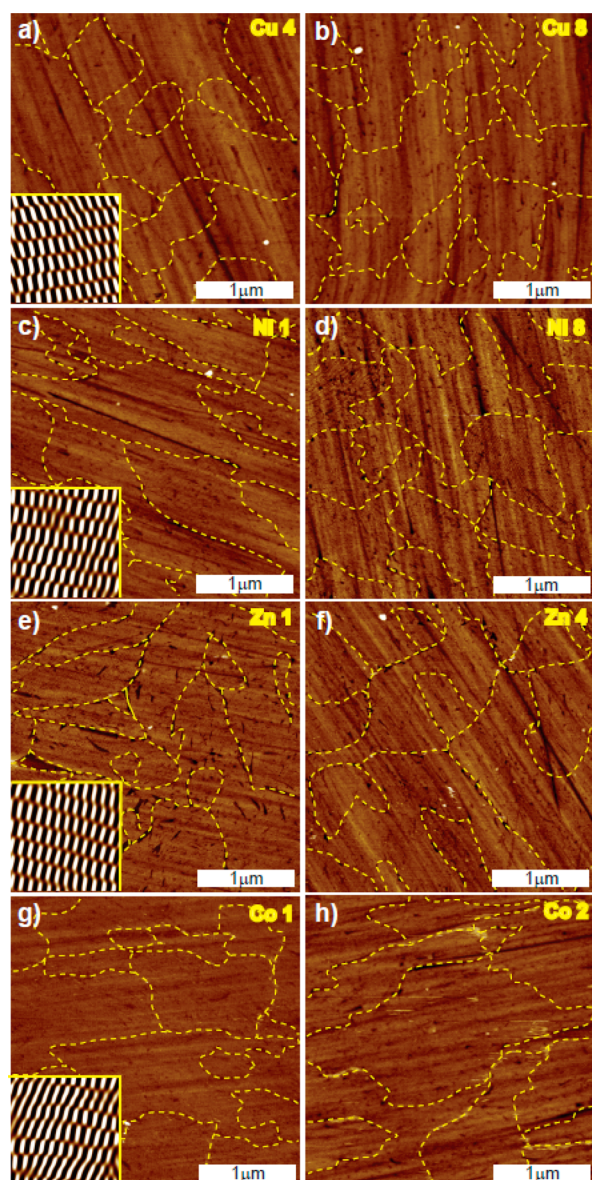
Figure 3. Typical AFM images of copper ion doped DNA lattices with ion concentrations of 4 and 8 mM denoted as Cu4 and Cu8 (a and b); nickel ion doped DNA lattices with 1 and 8 mM denoted as Ni1 and Ni8 (c and d); zinc ion doped DNA lattices with 1 and 4 mM denoted as Zn1 and Zn4 (e and f); and cobalt ion doped DNA lattices with 1 and 2 mM denoted as Co1 and Co2 (g and h), respectively. The yellow dotted lines in the AFM images indicate the DX DNA lattice domain boundaries. The insets in (a, c, e, and g) are the noise-filtered 2D spectrum images with a scan size 80 nm × 80 nm and show the periodicity of the metal ion doped DNA lattices.

bottom left in Figures 3(a, c, e, and g) are the noise-filtered 2D spectrum images according to fast Fourier transform and show the periodicity of the unit building block (DX tile). The surface morphologies of M−DNA complexes show that, even at higher metal ion concentrations, the topographical features are similar to those found in the DX lattices without metal ions.

The configuration of the metal ions within the DNA molecules is most likely intercalated between the base pairs and bound with the phosphate backbone sites. Eichhorn et al.[21] suggest that the metal ion binding sites in the DNA molecule are either phosphate groups or electron donor atoms on the heterocyclic bases. This report claims that if the metal ions are

binding with phosphate sites then the DNA helical property becomes stabilized. Conversely, if the metal ions are intercalated between base pairs the DNA helical property becomes destabilized. In most M−DNAs, the valence of the metal ions is two. This corresponds to the simple ion exchange by a divalent metal in place of two Na^+ counter cations for (PO_4^-) anions. When zinc ions in Zn^{2+}−DNA complexes are prepared by a freeze-drying method, possible electronic states of Zn^{2+} include covalent bonding of Zn^{2+} with the nitrogen atoms of the base pairs under extremely dry conditions.[22] Lee et al.[23] reported an M−DNA with divalent metal ions that were intercalated between the base pairs. In addition, one to five Cu^{2+}-mediated base pairs of hydroxypyridone nucleobases were systematically incorporated into the middle of a DNA duplex in the solution phase. This resulted in the formation of a magnetic chain as the Cu^{2+} in each complex lined up and coupled ferromagnetically through unpaired d electrons.[24]

The optical band gap is the optical threshold energy for HOMO−LUMO transition (see schematic band diagram of the optical transitions shown in Figure 1). Carriers excited across this gap may not have sufficient energy to reach the conduction band. This gap is smaller than the true HOMO−LUMO energy (namely, the energy band gap) by an exciton binding energy. Carriers excited across the energy band gap can carry currents. In many organic molecules, this is very difficult to measure directly, but it approaches the second absorption band. Practically, carriers excited to the second absorption band rapidly decay to the bottom of the conduction band, so that the onset of the second absorption band can be essentially taken to be the energy band gap as far as electrical transport measurements are concerned.

In order to extract the HOMO−LUMO or optical band gap from the transmittance spectra of the DX lattices modified by Cu^{2+}, Ni^{2+}, Zn^{2+}, or Co^{2+}, VUV (Visible−Ultraviolet) spectrophotometry was employed at ambient temperature and pressure. The fundamental absorption bands associated with the optical band gap presented in Figure 4 are characteristic of an electronic transition from π to π*. This is essentially a superposition of the corresponding HOMO−LUMO transitions in a simple DNA duplex. However, for this simple duplex in the solid phase, the HOMO−LUMO transitions are positioned in the energy range between 4.3 and 4.5 eV. Figures 4(a−d) present absorption coefficients $\alpha(E)$ as a function of energy E for the four aforementioned M−DNAs with various metal ion concentrations. There is a large, linear background in the VUV spectra caused by the substrate which was subtracted from all of our data before analysis. The pristine DNA DX lattice sample (labeled as DNA in Figures 4(a−d)) exhibits a clear optical band gap of 4.69 eV. For M−DNA complexes, the corresponding optical band gaps vary from 4.67 to 4.98 eV with different metal ion concentrations. The slight difference in band gap energies between the simple duplex DNA and the DX lattices is likely caused by the differences in the buffer environments, amorphous and crystalline natures, multistacking and single layers, and possible interfacial characteristics.[6,8,10,25] Therefore, we can assume that the M−DNA complexes interact less with their neighbors (single layered, 0.6 nm thick, in air) and are closer to their gas phase in this regard. Next to the fundamental absorption band is the low-energy tail of another strong absorption band. This comes from the superposition of the second absorption band of the DX lattice located at ~6 eV.
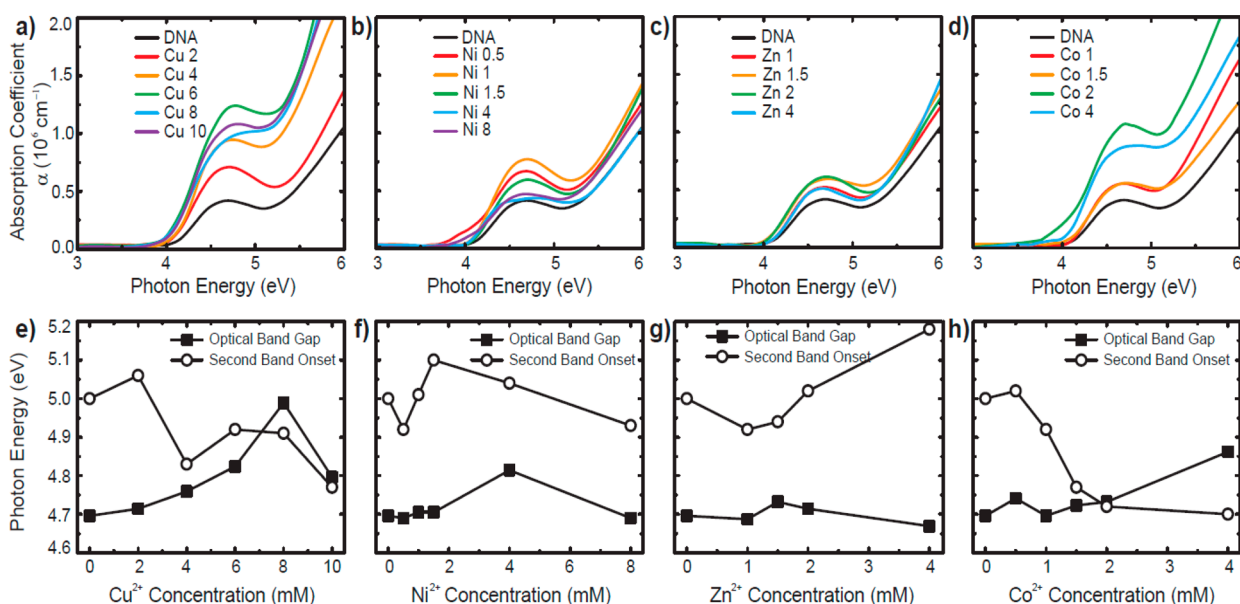
Figure 4. Analysis of the optical energy band gap as a function of the metal ion concentration in DX DNA polycrystalline lattices. The variation of the absorption coefficient as a function of photon energy for (a) Cu^{2+}–DNA, (b) Ni^{2+}–DNA, (c) Zn^{2+}–DNA, and (d) Co^{2+}–DNA. (e–h) Variation of the optical band gaps and second band onsets with various concentrations of Cu^{2+}, Ni^{2+}, Zn^{2+}, and Co^{2+} in the DX lattices.

In general, doping with metal ions initially shifts the optical band gaps to a higher energy, before decreasing again at higher concentrations and returning to a band gap close to the pristine DX lattice case. Here, we simply locate the energy of the local maximum and systematically present the doping dependence of the optical band gap for the four metal ion species that we considered (Figures 4(e–h)). The initial blue-shift of the optical band gap is consistent with the scenario where the doped metal ions act as a screen for the existing interaction between the DNA base pairs to the extent that the base pairs appear to approach their gas phase in terms of their optical characteristics. The gas phase corresponds to the larger HOMO–LUMO energy of free molecules. As the molecules condense into the solid phase, nearby molecules begin to interact with the HOMO–LUMO gap decreasing as a result. Our DX DNA lattices, in the form of monolayer film rather than multistacked assemblies, cause the molecules to interact rather weakly, and metal dopings also tend to separate the DNA molecules, moving the system toward the gas phase.[26] Beyond a critical doping concentration, overfilling of the metal ions begins to mediate nonspecifically between the DNA bases, eventually causing a red-shift in their optical band gap. This explains the bowing-shape (inverted 'V') behavior of the optical band gap as well as the associated critical doping level of M–DNA complexes. From observation of the Raman spectra (shown in the Supporting Information, Figure S2), the metal ions are intercalated between the base pairs and bound with the phosphate backbones up to a certain optimum doping ion concentration (C_o). In this scenario, they form long chains without disturbing the original DX lattices. Further doping with metal ions into the DX lattices causes the ions to bind to additional indeterminate sites, which in turn may produce stresses on the helical structure of the DNA lattices. If we anneal DX lattices on a substrate with metal ions (concentration higher than C_o) at the beginning, we do see the aggregated and amorphous formation of DNA molecules without periodicity in the DX lattices (Supporting Information, Figure S3). In contrast, when we added metal ions after

annealing the DX lattices on a substrate, we did not observe any structural disorders, even at slightly higher metal doping levels than C_o (Figure 3). In this scenario, the DX lattices might be experiencing physical stresses at the molecular level, but due to the strong electrostatic binding between a substrate and DX lattices, their structure appeared to be unaffected. The critical doping level, C_o, observed in our optical data likely corresponds to this structural transition point.

Figures 4(e–h) show the onset energies of the second optical absorption bands, which evolve with doping in a way that contrasts with the evolution of the optical band gaps. In general, this onset initially decreases before later increasing. However, we noticed that there is certain uncertainty in locating the onsets through linear fitting from the low-energy side of the second band gap; this is taken into account when analyzing the data. The evolution of these onsets is actually more consistent with our electrical (I–V) characteristics. We observed that I increases with increasing metal ion concentrations until C_o and then decreases as the ion concentration continues to increase (Supporting Information, Figure S4). At the C_o of all of the M–DNA complexes presented here, the metal ions optimally occupied their proper sites (base pairs and phosphate backbones) in the DX lattices and formed long chains inside the DNA duplexes. However, above the C_o, the metal ions were bound to nonspecific, undesignated sites of the DNA molecules. This caused stresses which influenced the helical structure and the curvature of the DNA duplexes. It should be pointed out that when discussing electrical transport characteristics the energy band gap is more relevant than the optical band gap. The optical band gap represents the minimum energy required to form an electron–hole pair, i.e., an exciton; this two-body state cannot directly participate in the transport process, which requires free electron–hole pairs. In contrast, the onset energy of the second optical absorption band is likely higher than the energy band gap (the true transport gap). Electron–hole pairs excited to this band can immediately undergo intraband transitions to the bottom of the conduction band and form current-carrying states. These types

of situations are commonly found in well-known organic semiconductors such as pentacene.[27,28] Remarkably, the onset energy of the second optical absorption band also exhibits a restoration pattern (except for the Co^{2+} case where the critical doping level was never reached). Our structural and optical investigations demonstrate that a metal ion doping can serve as an effective means to control the optical band gap energy and possibly the energy or transport band gap of M–DNA complexes with additional degrees of freedom in the metal ion species. All of these variables combine to critically affect the electronic and optical properties of the M–DNA complexes.

4. CONCLUSION

We have constructed 2D M–DNA complexes on fused silica by the SAG method. Initially, we estimated the percentage of lattice coverage as a function of DNA monomer concentration on substrate. We also discussed the band gaps of the M–DNA complexes with various metal ion concentrations. The HOMO–LUMO band gap of M–DNA complexes showed an inverted "V" shape. The second band onset, which is more consistent with the electrical characteristics, showed a similar "V" shape behavior which scaled with the metal ion concentration. The crossover point indicates the C_o for each metal ion in the DX lattices. This point may represent the optimum conditions for device performance. On the basis of our results, we concluded that metal ion doping is an effective method to tune the band gap energy of DNA-based nanostructures. Combined with the existing structural versatility of DNA nanostructures, this functional tunability will be crucial to the future development of DNA-based nanoelectronic devices and bioelectronic sensors.

■ ASSOCIATED CONTENT

ⓢ Supporting Information

Schematic diagram, sequence pool, and sticky-ends of the DX tiles used in this experiment, Raman, AFM images, and I–V characteristics. This material is available free of charge via the Internet at http://pubs.acs.org.

■ AUTHOR INFORMATION

Corresponding Authors
*E-mail: super@yonsei.ac.kr.
*E-mail: sunghapark@skku.edu.
Author Contributions
§These authors contributed equally to this work.
Notes
The authors declare no competing financial interest.

■ ACKNOWLEDGMENTS

■ REFERENCES

(1) Seeman, N. C. Nanomaterials Based on DNA. Annu. Rev. Biochem. 2010, 79, 65–87.

(2) Yin, P.; Hariadi, R. F.; Sahu, S.; Choi, H. M.; Park, S. H.; Labean, T. H.; Reif, J. H. Programming DNA Tube Circumferences. Science 2008, 321, 824–826.

(3) Winfree, E.; Liu, F.; Wenzler, L. A.; Seeman, N. C. Design and Self-Assembly of Two-Dimensional DNA Crystals. Nature 1998, 394, 539–544.

(4) He, Y.; Ye, T.; Su, M.; Zhang, C.; Ribbe, A. E.; Jiang, W.; Mao, C. Hierarchical Self-Assembly of Symmetric Supramolecular Polyhedra. Nature 2008, 452, 198–201.

(5) Rothermund, P. W. K. Folding DNA to Create Nanoscale Shapes and Patterns. Nature 2006, 440, 297–302.

(6) Gullu, O.; Cankaya, M.; Baris, O.; Biber, M.; Ozdemir, H.; Gulluce, M.; Turut, A. DNA-Based Organic-on-Inorganic Semiconductor Schottky Structures. Appl. Surf. Sci. 2008, 254, 5175–5180.

(7) Bhalla, V.; Bajpai, R. P.; Bharadwaj, L. M. DNA Electronics. EMBO Rep. 2003, 4, 442–445.

(8) Gullu, O.; Cankaya, M.; Baris, O.; Turut, A. DNA-Modified Indium Phosphide Schottky Device. Appl. Phys. Lett. 2008, 92, 212106.

(9) Sonmezoglu, S.; Sonmezoglu, O. A. Optical and Dielectric Properties of Double Helix DNA Thin Films. Mater. Sci. Eng., C 2011, 31, 1619–1624.

(10) Endress, R. G.; Cox, D. L.; Singh, R. R. P. The Quest for High-Conductance DNA. Rev. Mod. Phys. 2004, 76, 195–214.

(11) Iguchi, K. Semiconductivity and Band Gap of a Double Strand of DNA. J. Phys. Soc. Jpn. 2001, 70, 593–597.

(12) Tran, P.; Alavi, B.; Gruner, G. Charge Transport Along the DNA Double Helix. Phys. Rev. Lett. 2000, 85, 1564–1567.

(13) Zhang, Y.; Austin, R. H.; Kraeft, J.; Cox, E. C.; Ong, N. P. Insulating Behavior of DNA on the Micron Scale. Phys. Rev. Lett. 2002, 89, 198102.

(14) Cuniberti, G.; Craco, L.; Porath, D.; Dekker, C. Backbone-Induced Semiconducting Behavior in Short DNA Wires. Phys. Rev. B 2002, 65, 241314.

(15) Porath, D.; Bezryadin, A.; de Vries, S.; Dekker, C. Direct Measurement of Electrical Transport Through DNA Molecules. Nature 2000, 403, 635–638.

(16) Hamada, S.; Murata, S. Substrate-Assisted Assembly of Interconnected Single-Duplex DNA Nanostructures. Angew. Chem., Int. Ed. 2009, 48, 6820–6823.

(17) Lee, J.; Kim, S.; Kim, J.; Lee, C. W.; Roh, Y.; Park, S. H. Coverage Control of DNA Crystals Grown by Silica Assistance. Angew. Chem., Int. Ed. 2011, 50, 9145–9149.

(18) Dugasani, S. R.; Kim, J. A.; Kim, B.; Rao, P. J.; Gnapareddy, B.; Vyas, C.; Kim, T. S.; Park, S. H.; Manchanda, V. A 2D DNA Lattice as an Ultra-Sensitive Detector for Beta Radiations. ACS Appl. Mater. Interfaces 2014, 6, 2974–2979.

(19) Liu, H.; He, Y.; Ribbe, A. E.; Mao, C. Two-Dimensional (2D) DNA Crystals Assembled from Two DNA Strands. Biomacromolecules 2005, 6, 2943–2945.

(20) Dugasani, S. R.; Lee, N. H.; Lee, J.; Kim, B.; Hwang, S. U.; Lee, K. W.; Kang, W. N.; Park, S. H. Magnetic Characteristics of Copper Ion-Modified DNA Thin Films. Sci. Rep. 2013, 3, 1819.

(21) Eichhorn, G. L.; Marzilli, L. G. Advances in Inorganic Biochemistry; Elsevier: New York, 1982.

(22) Omerzu, A.; Anzelak, B.; Turel, I.; Strancar, J.; Potocnik, A.; Arcon, D.; Arcon, I.; Mihailvic, D.; Matsui, H. Strong Correlations in Highly Electron-Doped Zn(II)-DNA Complexes. Phys. Rev. Lett. 2010, 104, 156804.

(23) Lee, J. S.; Latimer, L. J. P.; Reid, R. S. A. Cooperative Conformational Change in Duplex DNA Induced by Zn^{2+} and Other Divalent Metal Ions. Biochem. Cell Biol. 1993, 71, 162–168.

(24) Tanaka, K.; Tengeiji, A.; Kato, T.; Toyama, N.; Shionoya, M. A. Discrete Self-Assembled Metal Array in Artificial DNA. Science 2003, 299, 1212–1213.

(25) Sönmezoğlu, S.; Sönmezoğlu, Ö.A.; Çankaya, G.; Yildirim, A.; Serin, N. Electrical Characteristics of DNA-Based Metal-Insulator-Semiconductor Structures. J. Appl. Phys. 2010, 107, 124518–6.

(26) Silaghi, S. D.; Friedrich, M.; Cobet, C.; N. Esser, N.; Braun, W.; Zahn, D. R. T. Dielectric Functions of DNA Base Films from Near-Infrared to Ultra-Violet. Phys. Status Solidi (B) 2005, 242, 3047–3052.

(27) Lee, J.; Kim, S. S.; Kim, K.; Kim, J. H.; Im, S. Correlation Between Photoelectric and Optical Absorption Spectra of Thermally Evaporated Pentacene Films. *Appl. Phys. Lett.* **2004**, *84*, 1701.

(28) Kim, S. S.; Park, S. P.; Kim, J. H.; Im, S. Photoelectric and Optical Properties of Pentacene Films Deposited on n-Si by Thermal Evaporation. *Thin Solid Films* **2002**, *420−421*, 19−22.